

# Modeling gross primary production of maize cropland and degraded grassland in northeastern China

Zheng Wang<sup>a,b</sup>, Xiangming Xiao<sup>c</sup>, Xiaodong Yan<sup>a,\*</sup>

<sup>a</sup> Key Laboratory of Regional Climate-Environment Research for Temperate East Asia, Institute of Atmospheric Physics, Chinese Academy of Sciences, Beijing 100029, China

<sup>b</sup> Graduate University of the Chinese Academy of Sciences, Beijing 100049, China

<sup>c</sup> Department of Botany and Microbiology, Center for Spatial Analysis, University of Oklahoma Norman, Oklahoma 73019-5300, USA

## ARTICLE INFO

### Article history:

Received 14 May 2009

Received in revised form 23 April 2010

Accepted 23 April 2010

### Keywords:

Vegetation Photosynthesis Model

CO<sub>2</sub> fluxes

Light use efficiency

Semi-arid grassland

## ABSTRACT

Measurements from individual CO<sub>2</sub> eddy flux sites provide valuable information on the seasonal dynamics of gross primary production (GPP). In this study, we estimated seasonal dynamics of GPP from 3 years (2004–2006) of the eddy covariance observations at maize cropland and degraded grassland in a semi-arid area of Tongyu county (44.5667°N, 122.8833°E), Northeast China. The biophysical performance of vegetation indices (EVI, NDVI, and LSWI) derived from the 8-day Moderate Resolution Imaging Spectroradiometer (MODIS) surface reflectance product and their relations to GPP dynamics were evaluated. The quantitative relationships between the vegetation indices and CO<sub>2</sub> flux data clearly demonstrated the improvement of EVI over NDVI, in terms of the phase and magnitude of photosynthesis. Canopy-level maximum light use efficiency,  $\epsilon_0$ , was estimated for both maize and grassland by using the observed CO<sub>2</sub> flux data and Photosynthetically Active Radiation (PAR) data from eddy flux tower sites. For maize cropland, the  $\epsilon_0$  value was 0.56 gC/mol PAR, and for degraded grassland, the  $\epsilon_0$  value was 0.37 gC/mol PAR. We conducted a simulation of the Vegetation Photosynthesis Model (VPM) using the Enhanced Vegetation Index (EVI) and the Land Surface Water Index (LSWI) derived from the 8-day (MODIS) surface reflectance product, as well as site-specific climate data. The comparison between simulated GPP and estimated GPP from tower CO<sub>2</sub> flux data showed good agreement in both maize cropland and degraded grassland. This study highlighted the biophysical performance of improved vegetation indices in relation to GPP and demonstrated the potential of the satellite-driven VPM model for scaling-up of GPP of maize cropland and grassland in semi-arid ecosystems.

© 2010 Elsevier B.V. All rights reserved.

## 1. Introduction

The terrestrial biosphere is an integral part of the global carbon cycle. Every year about 14% of the carbon in the atmosphere is exchanged with the terrestrial biosphere (Friend et al., 1997; Wesfall and Stumm, 1980). Arid and semi-arid regions make up between 30% and 45% of the global terrestrial surface (Evenari et al., 1985; Verhoef et al., 1999). These regions are important with respect to land-atmosphere interactions because of their unique energy budget (high sensible heat flux) and increasing aridification and desertification (Fu and Wen, 2002; Fu and An, 2002; Laura and Huenneke, 2002). However, land surface-atmosphere processes in arid and semi-arid areas have received much less attention in comparison with other regions (Baldocchi et al., 2001; Elmar and Veenendaal, 2004; Goodrich et al., 2000). Arid and semi-arid landscapes cover more than one-third of China (Liu et al., 2008). Most

early research in those semi-arid and arid regions of China focused on intensive field-observation periods of 2 months, for example, HEIFE (Hu and Gao, 1994; Wang and Mitsuta, 1991), IMGRASS (Lu et al., 2005), GAME/Tibet, CAMP/Tibet, TIPEX98 (Ma et al., 2006; Xu et al., 2002) and the Dunhuang experiment (Zhang et al., 2001).

The eddy covariance technique is one of the advanced micrometeorological methods for estimating CO<sub>2</sub>, water, and energy exchanges between the atmosphere and terrestrial ecosystems (Baldocchi et al., 2001; Wofsy et al., 1993). According to FLUXNET (<http://www.fluxnet.ornl.gov/fluxnet/index.cfm>), over 500 tower sites presently operate on a long-term and continuous basis. Vegetation types represented include temperate conifer and broadleaf (deciduous and evergreen) forests, tropical and boreal forests, crops, grasslands, chaparral, wetlands, and tundra. Data compiled from flux towers are being used to quantify and compare magnitudes and dynamics of annual ecosystem carbon and water balances, to quantify the response of stand-scale carbon dioxide and water vapor flux densities in controlling biotic and abiotic factors, and to validate a hierarchy of soil–plant–atmosphere trace gas exchange models (Baldocchi et al., 2001).

\* Corresponding author. Tel.: +86 010 82995136.

E-mail addresses: [yxd@tea.ac.cn](mailto:yxd@tea.ac.cn), [yxd@mail.tea.ac.cn](mailto:yxd@mail.tea.ac.cn) (X. Yan).

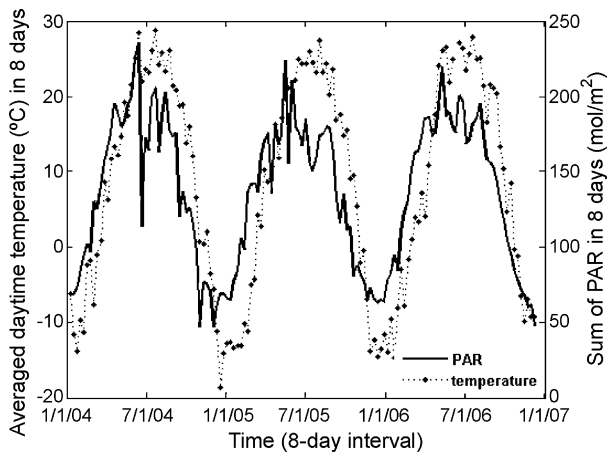


**Fig. 1.** The seasonal dynamics of Photosynthetically Active Radiation (PAR) and averaged daytime temperature from 2004 to 2006 at the two semi-arid ecosystems: cropland and degraded grassland in Tongyu, northeastern China.

Recently, many studies have used site-specific net ecosystem exchange of  $\text{CO}_2$  (NEE) and satellite observations for vegetation photosynthesis analysis and gross primary production (GPP) modeling. Examples of these models are the URC, MODIS-PSN, and GLO-PEM (Goetz et al., 1999; Heinsch et al., 2003; Ruimy et al., 1996). The satellite-based Vegetation Photosynthesis Model (VPM) was recently developed (Xiao et al., 2002, 2005a, 2004a, 2004b, 2005b) to estimate light absorption by chlorophyll and GPP of terrestrial ecosystems, based on the concept that vegetation canopy is composed of chlorophyll and non-photosynthetically active vegetation (mostly senescent foliage, stems, and branches). The potential of the VPM model for scaling-up GPP has been evaluated for  $\text{CO}_2$  flux tower sites in forest (temperate deciduous broadleaf forest, evergreen coniferous forest, seasonally moist tropical forest) and alpine grassland (Xiao et al., 2002, 2005a, 2004a, 2004b, 2005b; Li et al., 2007). However, the VPM model has not been evaluated and applied in maize cropland and degraded grassland in semi-arid regions.

In this study, our objectives are: (1) to evaluate biophysical performance of vegetation indices (EVI, NDVI, LSWI) derived from MODIS in a semi-arid region; (2) to predict GPP with the VPM model by using climate data and MODIS imagery; and (3) to evaluate the potential of the VPM model for estimating GPP of maize cropland and degraded grassland in semi-arid regions.

## 2. The study sites and data

### 2.1. A brief description of the study sites

The study sites are located in a semi-arid area of Tongyu county, Jilin Province, northeastern China. The terrain in this area is fairly open and flat with a terrain slope of less than  $1^\circ$ . It has a semi-arid continental climate of the mid-temperate zone, dominated by the southeast monsoon in summer and high pressure from Siberia in winter. The annual mean air temperature of the most recent 30-year period is  $5.5^\circ\text{C}$ , with a range from  $-33.7^\circ\text{C}$  to  $38.9^\circ\text{C}$ . The seasonal dynamics of 8-day-averaged daytime temperature for 2004–2006 are shown in Fig. 1. Annual precipitation ranged from 206.8 mm to 606.7 mm with a mean of 345.4 mm, and approximately 80% of annual rainfall occurs from May to September. The study area is covered by light chernozem and meadow slouchaks mainly.

The degraded grassland, which was classified as temperate *Leymus chinensis* meadow before degradation by livestock overgrazing, is now covered largely by *chloris virgata* community and

annual weed community, which present a spatially random distribution. *Chloris virgata* community is distributed over relatively higher elevation areas while annual weed community inhabits lower elevation sites. *Leymus chinensis* plants are visible on occasion. Grass can reach a maximum height of 10 cm during the plant-growing season.

The cropland is located 2-km north of Xinhua town with no obstacles found within 2-km and sporadic forest belts in farmlands beyond the 2 km. The main crop is maize within 1000 m of the measurement location in the cropland ecosystem during the growing season, while in winter there is bare soil. The maximum height of the maize is near 1.8 m during the growing season. The maize is usually sown by late April to early May and harvested at the end of September or at the beginning of October, but harvest also depends on the beginning of the rainy season in each year. There are no rivers within this area. Irrigation does occur during the sown period based on the farmer's cultivation practices, but plant growth is mainly dependent on precipitation (Liu et al., 2008).

### 2.2. A brief description of $\text{CO}_2$ eddy flux measurement

As part of a long-term field experiment on aridification and human activity in a semi-arid region, two eddy covariance flux towers were established in the two ecosystems of the Tongyu station, Jilin Province in October of 2002, a maize cropland site ( $44.5673^\circ\text{N}$ ,  $122.92^\circ\text{E}$ ) and a degraded grassland site ( $44.5913^\circ\text{N}$ ,  $122.52^\circ\text{E}$ ).

The eddy covariance flux observation system consists of an ultrasonic anemometer/thermometer (CSAT3, Campbell Scientific Ltd, USA) and LI-7500 Li-Cor open path  $\text{CO}_2/\text{H}_2\text{O}$  analyzer and has been operating continuously to measure  $\text{CO}_2$ ,  $\text{H}_2\text{O}$ , and energy fluxes half-hourly since October of 2002. The measured height of the EC system on maize cropland and degraded grassland is at 2 m and 3.5 m respectively. Momentum, sensible heat, water vapor, and  $\text{CO}_2$  fluxes were calculated at an averaging time of 30 min in post-processing from the 10 Hz time series raw data. With instrument malfunction, weather condition, and calibration issues, high quality data comprises 70% to 80% of data obtained during any 1 year. Flux footprint analysis indicates that approximately 85% of the measured scalar flux originates within 600 m of the tower (Liu et al., 2008).

Tongyu station is a site of the long-term field experiment on aridification and human activity in semi-arid regions (<http://observation.tea.ac.cn>) and is also a reference site of CEOP (Coordinate Energy and Water Cycle Observations Project) (<http://monsoon.t.u-tokyo.ac.jp/ceop2/>). A data management staff in the RCE-TEA (Key Laboratory of Regional Climate-Environment Research for Temperate East Asia, Chinese Academy of Sciences) is in charge of data quality control and gap filling. To fill missing and bad data, a linear interpolation method was used for small blocks (less than a few hours) of missing or bad data. Larger gaps were filled with values derived from mean diurnal ensemble values (Falge et al., 2001a; Falge et al., 2001b). Gaps in precipitation were filled using data from the weather station at Tongyu County, 30 km northeast of the observation sites (Liu et al., 2008). The data set used in this study is available from the previously mentioned websites. This data set contains the Coordinated Enhanced Observing Periods 3 and 4 (EOP-3 and EOP-4) CEOP Asia-Australia Monsoon Project (CAMP). Liu et al. (2008) analyzed 3-year variations of water, energy and  $\text{CO}_2$  fluxes of cropland and degraded grassland surfaces based on the dataset. Jiang et al. (2007) conducted a comparison between simulated land surface fluxes and observed eddy covariance measurements.

Gross primary production (GPP) was estimated, using site-specific  $\text{CO}_2$  flux and climate data. The first step was to estimate ecosystem respiration. All half-hourly  $\text{CO}_2$  flux data points with PAR values  $<5 \mu\text{mol}/\text{m}^2/\text{s}$  were used as nighttime NEE, so NEE data

were partitioned into a light-dependent part (daytime NEE) and a light-independent part (nighttime NEE). The nighttime NEE data were used to estimate  $R_{\text{night}}$  (nighttime respiration rate).  $R_{\text{day}}$  (daytime ecosystem respiration) was determined from the relationships between nocturnal ecosystem respiration and air temperature (2 m height) using the Van't-Hoff function.

$$NEE_{\text{night}} = R_{\text{ref},10} \times Q_{10}^{(T-10)/10} \quad (1)$$

For each month, all nighttime NEE values were regressed against measured air temperature (2 m height) using Eq. (1). The resulting regression equation was then used with measured air temperatures (2 m height) to predict  $R_{\text{day}}$ . GPP was then estimated as NEE minus ecosystem respiration (Xiao et al., 2004a), using the convention of opposite signs for GPP and ecosystem respiration. We calculated 8-day sums of GPP from the daily data, to be temporally consistent with the 8-day composite MODIS satellite images (Fig. 5).

### 2.3. 8-Day composite images from MODIS sensor

The MODIS sensor acquires images in 36 spectral bands ranging from 0.4  $\mu\text{m}$  to 14.4  $\mu\text{m}$ . Of the 36 spectral bands, seven bands are designed for the study of vegetation and land surfaces: blue (459–479 nm), green (545–565 nm), red (620–670 nm), NIR (841–875 nm, 1230–1250 nm), and SWIR (1628–1652 nm, 2105–2155 nm). The MODIS Land Science Team provides several data products derived from MODIS observations to the public, including the 8-day composite Land Surface Reflectance (MOD09A1). The MOD09A1 datasets include seven spectral bands mentioned above at a spatial resolution of 500-m, and have been corrected for the effects of atmospheric gases, aerosols, and thin cirrus clouds. The MOD09A1 datasets are provided to users in a tile mode, and each tile covers  $10^\circ$  latitude by  $10^\circ$  longitude.

In this study, we downloaded images for January 2004 to December 2006 and extracted land surface reflectance data of MODIS pixels, based on the geo-location information (latitude and longitude) of these two eddy covariance flux tower sites in Tongyu station. An earlier study used time series MODIS data from one MODIS pixel,  $3 \times 3$  MODIS pixels and  $5 \times 5$  MODIS pixels for analysis of vegetation indices and simulation of the VPM model at a forest eddy flux tower site, and the results indicated that the results are not significantly different (Xiao et al., 2005a; Xiao et al., 2005b), so we only report the data from one pixel (500 m  $\times$  500 m) in this study.

Land surface reflectance values from four spectral bands (blue, red, NIR (841–875 nm) and SWIR (1628–1652 nm)) were used to calculate three vegetation indices: the Normalized Difference Vegetation Index (NDVI, Tucker, 1979), the Enhanced Vegetation Index (EVI, Huete et al., 1997), and the Land Surface Water Index (LSWI, Xiao et al., 2004a).

$$NDVI = \frac{\rho_{\text{nir}} - \rho_{\text{red}}}{\rho_{\text{nir}} + \rho_{\text{red}}} \quad (2)$$

$$LSWI = \frac{\rho_{\text{nir}} - \rho_{\text{swir}}}{\rho_{\text{nir}} + \rho_{\text{swir}}} \quad (3)$$

$$EVI = 2.5 \times \frac{\rho_{\text{nir}} - \rho_{\text{red}}}{\rho_{\text{nir}} + 6 \times \rho_{\text{blue}} - 7.5 \times \rho_{\text{red}} + 1} \quad (4)$$

where  $\rho_{\text{nir}}$ ,  $\rho_{\text{red}}$ ,  $\rho_{\text{swir}}$ ,  $\rho_{\text{blue}}$  are reflectances of the near infrared, red, shortwave infrared and blue bands, respectively.

NDVI (Tucker, 1979) has been widely used in describing terrestrial vegetation, but it suffers from several limitations. When dealing with low vegetation coverage, it seems that NDVI cannot identify vegetation from soil background with a high precision. EVI (Huete et al., 1997) includes the blue band for atmospheric correction, and it works well in accounting for residual atmospheric contamination (e.g. aerosols), variable soil, and canopy background

reflectance. EVI has been recently used for the study of temperate forests, seasonally moist tropical forest, evergreen coniferous forest and alpine grassland (Xiao et al., 2005a; Xiao et al., 2004a; Xiao et al., 2004b; Xiao et al., 2005b; Li et al., 2007). Calculated as the normalized difference between NIR and SWIR spectral bands, LSWI (Xiao et al., 2004a) was used to characterize water conditions of vegetation in this study.

## 3. The Vegetation Photosynthesis Model (VPM)

### 3.1. Model framework

The VPM model is based on the concept that leaves and canopy are composed of photosynthetically active vegetation (mostly chlorophyll) and non-photosynthetic vegetation (NPV). Thus the Fraction of Absorbed Photosynthetically Active Radiation (FPAR) is partitioned into the fraction absorbed by chlorophyll (FPAR<sub>chl</sub>) and the fraction absorbed by NPV (FPAR<sub>NPV</sub>). Note that only the FPAR<sub>chl</sub> is used for photosynthesis. GPP can be described by:

$$GPP = \varepsilon_g \times FPAR_{\text{chl}} \times PAR \quad (5)$$

$$FPAR_{\text{chl}} = \alpha \times EVI \quad (6)$$

$$\varepsilon_g = \varepsilon_0 \times T_{\text{scalar}} \times W_{\text{scalar}} \times P_{\text{scalar}} \quad (7)$$

where  $\varepsilon_g$  is the light use efficiency (g C/mol PAR), PAR is the Photosynthetically Active Radiation ( $\mu\text{mol}/\text{m}^2/\text{s}$ , photosynthetic photon flux density, PPFD), FPAR<sub>chl</sub> is the fraction of PAR absorbed by chlorophyll; EVI is Enhanced Vegetation Index,  $\alpha$  is the coefficient in the EVI-FPAR<sub>chl</sub> linear function;  $\varepsilon_0$  is the maximum light use efficiency (g C/mol PAR), and  $T_{\text{scalar}}$ ,  $W_{\text{scalar}}$ , and  $P_{\text{scalar}}$  are the down-regulation scalars for the effects of temperature, water, and leaf phenology on the light use efficiency of vegetation, respectively. The VPM model uses EVI to estimate FPAR<sub>chl</sub>, with the coefficient  $\alpha$  being set to 1 (Xiao et al., 2004a).

The parameter  $\varepsilon_g$  is estimated as a function of the maximum light use efficiency ( $\varepsilon_0$ ) and down-regulation factors ranging between 0 and 1:  $T_{\text{scalar}}$ ,  $W_{\text{scalar}}$ , and  $P_{\text{scalar}}$ :

$$T_{\text{scalar}} = \frac{(T - T_{\text{min}})(T - T_{\text{max}})}{[(T - T_{\text{min}})(T - T_{\text{max}})] - (T - T_{\text{opt}})^2} \quad (8)$$

$$W_{\text{scalar}} = \frac{1 + LSWI}{1 + LSWI_{\text{max}}} \quad (9)$$

$$P_{\text{scalar}} = \frac{1 + LSWI}{2} \quad (10)$$

where  $T_{\text{scalar}}$  accounts for effects of temperature on canopy photosynthesis, using the equation developed for the Terrestrial Ecosystem Model (Raich et al., 1991);  $T_{\text{min}}$ ,  $T_{\text{max}}$ , and  $T_{\text{opt}}$  are the minimum, maximum and optimum temperature for photosynthetic activities, respectively;  $W_{\text{scalar}}$  represents the effect of water on plant photosynthesis with  $LSWI_{\text{max}}$  being the maximum LSWI value within the plant-growing season for each site (or pixel); and  $P_{\text{scalar}}$  accounts for effects of leaf age on canopy photosynthesis, using LSWI to identify the green-up and senescence phases. For deciduous vegetation,  $P_{\text{scalar}}$  is computed as a linear function of LSWI from bud burst to leaf full expansion, and after that it is set to 1. In this study we used Eq. (10) in maize cropland, and for grassland ecosystems  $P_{\text{scalar}}$  was set to 1 directly because grassland always has new leaves emerging during the plant-growing season (Xiao et al., 2004a).

### 3.2. Estimation of model parameters

In order to run the VPM model for estimating gross primary production of maize cropland and degraded grassland using MODIS

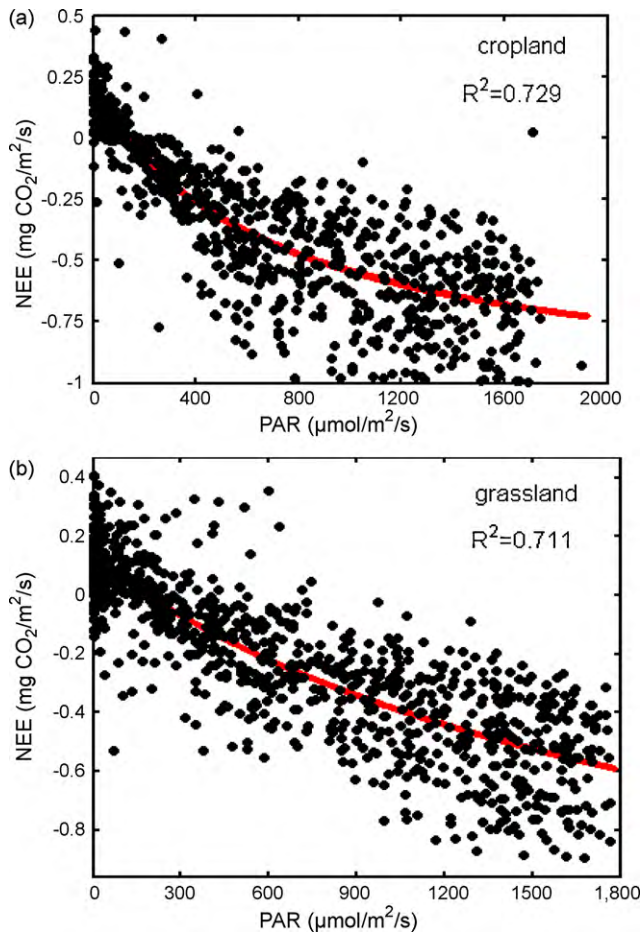


**Fig. 2.** The relationship between daytime net ecosystem exchange (NEE) of  $\text{CO}_2$  and Photosynthetically Active Radiation (PAR) in 2005 at (a) maize cropland and (b) degraded grassland. The two semi-arid ecosystems are in Tongyu, northeastern China.

imagery and climate data, we need to estimate four sets of parameters:

- (1) The maximum light use efficiency,  $\varepsilon_0$ , for maize cropland and degraded grassland: On average,  $\varepsilon_0$  has a value around  $1/6 \text{ g C/MJ}$  for well-watered, C3 plants at optimal temperatures (Mahadevan et al., 2008), but for a semi-arid area we need accurate information.  $\varepsilon_0$  can be obtained from analysis of net ecosystem exchange of  $\text{CO}_2$  and photosynthetic photon flux density (PPFD) at  $\text{CO}_2$  eddy flux tower sites (Ruimy et al., 1995). The estimation is largely determined by the choice of either a linear or nonlinear model over a year (Wofsy et al., 1993). In this study,  $\varepsilon_0$  was estimated for maize cropland and degraded grassland in semi-arid regions using a nonlinear hyperbolic model, the Michaelis–Menten function.

$$\text{NEE} = \frac{\varepsilon_0 \times \text{PAR} \times \text{GPP}_{\max}}{\varepsilon_0 \times \text{PAR} + \text{GPP}_{\max}} - R \quad (11)$$

where  $\varepsilon_0$  is apparent quantum yield,  $\text{GPP}_{\max}$  is the maximum estimated GPP from flux data, standing for maximum photosynthetic capacity, and  $R$  is ecosystem respiration. The resultant  $\varepsilon_0$  values are then used in the VPM model (see Eq. (7)). The fit curves are shown in Fig. 2. We used the daytime NEE and PAR within the peak period of the vegetation growing season (from July to August) in 2005 when the temperature and rainfall were optimal in the study period. The  $\varepsilon_0$  value for the maize crop-

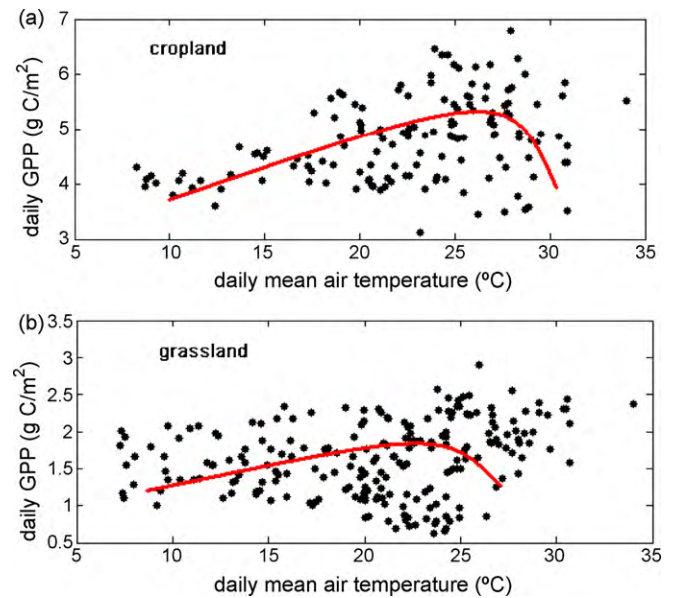


**Fig. 3.** The relationship between daily mean temperature and daily gross primary production at (a) maize cropland and (b) degraded grassland. The two semi-arid ecosystems are in Tongyu, northeastern China.

land was  $0.56 \text{ g C/mol PAR}$ , and the  $\varepsilon_0$  value for the degraded grassland was  $0.37 \text{ g C/mol PAR}$ .

- (2) The effect of temperature on plant photosynthesis ( $T_{\text{scalar}}$ ): Temperature affects GPP because sufficient, but not excessive, heat is a prerequisite for photosynthesis. Photosynthesis is restricted to a certain temperature range beyond which biological activity is inhibited. Within this range, photosynthesis increases up to an optimal temperature, beyond which it begins to decrease. The temperature range over which plants can photosynthesize is quite large. In calculation of  $T_{\text{scalar}}$ ,  $T_{\min}$ ,  $T_{\text{opt}}$  and  $T_{\max}$  values vary among different vegetation types. We picked out the limiting temperatures based on the relationship between temperature and photosynthesis and the analysis of VPM model testing. Fig. 3 shows the relationship between daily mean temperature and daily gross primary production. The daily GPP points were estimated from  $\text{CO}_2$  flux and climate data in 2005, when the temperature and rainfall were optimal in the study time (2004–2006). Daily mean temperatures were calculated by daily maximum air temperature and daily minimum air temperature. The curve came from Matlab curve fitting program. We can get optimum temperature ( $T_{\text{opt}}$ ) from the curve fitting. Photosynthesis is restricted to a certain temperature range, within this range, photosynthesis increases up to an optimal temperature, beyond which it begins to decrease. For degraded grassland we used a optimum temperature ( $T_{\text{opt}}$ ) of  $25^\circ\text{C}$ , for maize cropland we used  $26^\circ\text{C}$ .  $T_{\min}$  and  $T_{\max}$  came from the analysis of VPM model testing. For degraded grassland we used a minimum temperature ( $T_{\min}$ ) of  $-1^\circ\text{C}$ , and a maximum temperature ( $T_{\max}$ ) of  $35^\circ\text{C}$ ; for maize cropland we used  $-4$  and  $40^\circ\text{C}$  for  $T_{\min}$  and  $T_{\max}$ , respectively. We used daily maximum air temperature and daily minimum air temperature to calculate daily daytime mean temperature, instead of using the usual meteorological daily mean air temperature (Xiao et al., 2004a). If air temperature falls below  $T_{\min}$ ,  $T_{\text{scalar}}$  is set to be zero (Xiao et al., 2004a).
- (3) The effect of water on plant photosynthesis ( $W_{\text{scalar}}$ ): To calculate  $W_{\text{scalar}}$ , we need to estimate site-specific  $\text{LSWI}_{\max}$  (see Eq. (9)). We used the maximum  $\text{LSWI}$  value within the plant-growing season;  $\text{LSWI}$  values in winter are often affected by snow cover in winter and not used in the VPM model. The

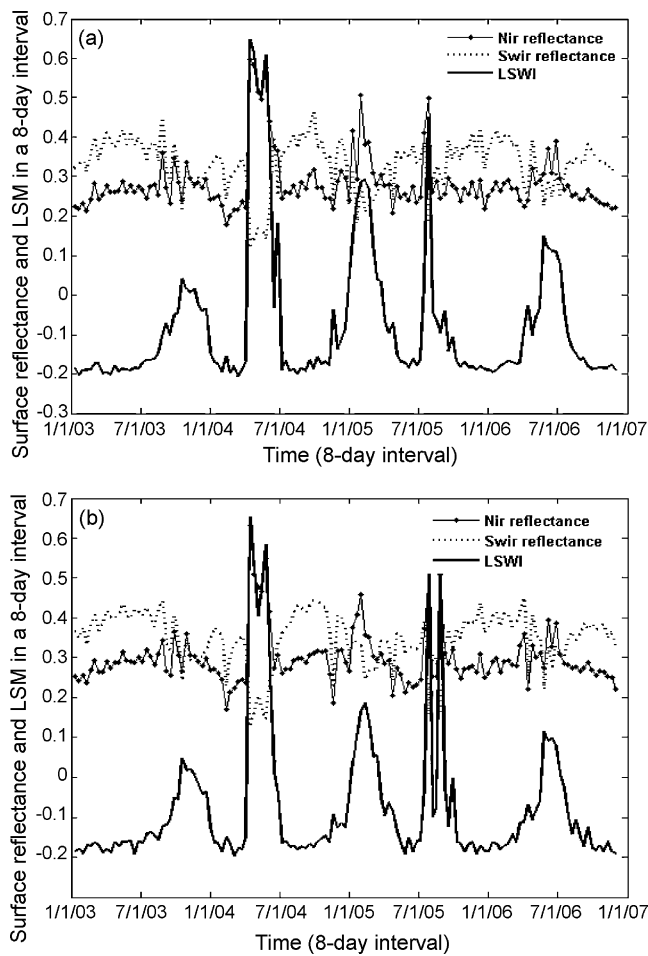


**Fig. 4.** The time series of surface reflectance of near infrared and shortwave infrared and Land Surface Water Index (LSWI) from 2004 to 2006 at (a) maize cropland and (b) degraded grassland. The two semi-arid ecosystems are in Tongyu, northeastern China.

$LSWI_{max}$  values were 0.29 and 0.19 for maize cropland and degraded grassland, respectively (Fig. 4).

- (4) The effect of leaf phenology (leaf age) on plant photosynthesis ( $P_{scalar}$ ): For grassland ecosystems that always have new leaves during the vegetation growing season,  $P_{scalar}$  is set to 1.0. For maize cropland it is computed as a linear function of LSWI from bud burst to leaf full expansion (see Eq. (10)), and after leaf full expansion it is set to be 1.0 (Xiao et al., 2004a).

## 4. Results and discussion

### 4.1. Temporal analyses of estimated GPP and meteorological data during 2004–2006

The GPP time series of both maize cropland and degraded grassland during 2004–2006 had a distinct seasonal cycle (Fig. 5), with obvious differences between them in phase and amplitude of the cycle. In degraded grassland, during winter days, photosynthetic activities were inhibited because of cold temperature and frozen soil. The estimated GPP values were zero. GPP increased gradually from March and reached its peak in late July to early August. After its peak, GPP declined in autumn and reached zero again in winter. Note that there were temporary depressions in late June to early July during 2004–2006, which were due to low temperature and low PAR during rainy days (Fig. 1).

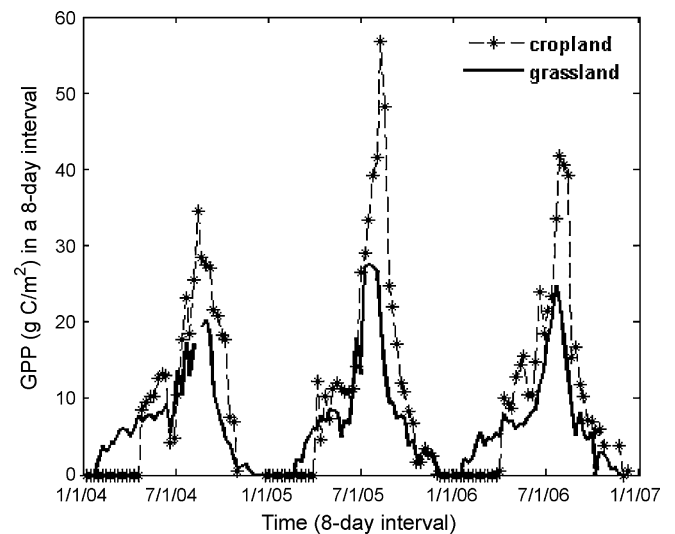


**Fig. 5.** The seasonal dynamics of gross primary production (GPP) from 2004 to 2006 at the two semi-arid ecosystems: cropland and degraded grassland in Tongyu, northeastern China.

Compared with the grassland site, the maize cropland site had similar seasonal dynamics with a peak in summer and trough in winter. GPP time series for maize cropland during 2004–2006 at Tongyu semi-arid region had a rapid rise and a sudden drop. GPP was always zero during winter, and increased rapidly in late April to early May. GPP continued increasing, reached its peak in late August to September, and declined rapidly after late September to early October. The similar GPP depression appeared in late June to early July because of rainy days.

The seasonal dynamics of GPP in degraded grassland can be partially explained by the season dynamics of temperature and PAR. However, the maize cropland was not a natural ecosystem and was affected by the farmer's cultivation practice (e.g. seeding and harvesting) in addition to climatic factors. As the maize cropland and the degraded grassland exist under the control of similar climatic conditions, we only present the main meteorological data of degraded grassland ecosystem in 2004–2006 (Fig. 1). The seasonal changes of GPP illustrate the timing of leaf emergence, peak leaf area and production, and leaf senescence and dormancy. In spring, as temperature warmed and the days became longer, grass foliage emerged, photosynthesis began, and GPP of grassland increased gradually. At the same time, GPP values of maize cropland were still zero until a rapid increase occurred in late April to early May after seeding. In autumn as leaves became senescent and dormant, GPP of grassland decreased gently, while maize cropland had a sudden drop after harvest. The rapid increase in spring and sudden drop in autumn for maize GPP is a good indicator of the planting and harvest dates.

### 4.2. Season dynamics of vegetation indices from MODIS sensor

Fig. 6 exhibits the seasonal dynamics of EVI and NDVI during 2004–2006 at the two semi-arid ecosystems in Tongyu, northeastern China. The EVI and NDVI curves were derived from the standard 8-day MOD09A1 surface reflectance products and mimicked the development and senescence of vegetation well. EVI and NDVI began to increase in spring and reached their maximum values during July to August, then started to decline and remained low in winter. In January of 2004 and 2005, EVI and NDVI values were both low. Compared with Fig. 4, the LSWI curve had reached the highest values at the same time. This was because snowfall occurred in winter; snow cover and icy soil changed the surface reflectance.

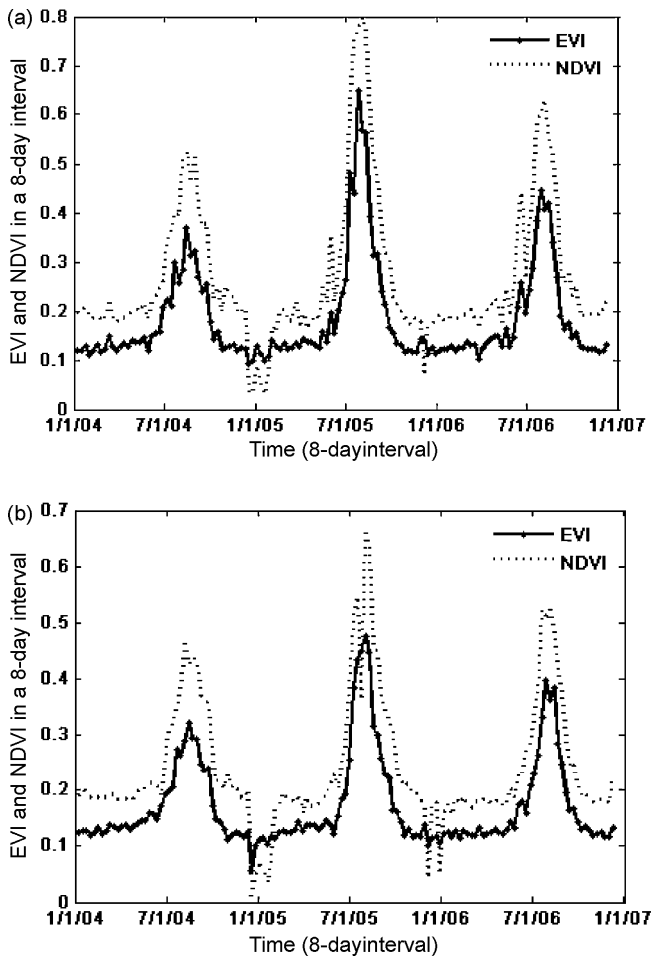


**Fig. 6.** The seasonal dynamics of Enhanced Vegetation Index (EVI) and Normalized Difference Vegetation Index (NDVI) during 2004–2006 at (a) maize cropland and (b) degraded grassland. The two semi-arid ecosystems are in Tongyu, northeastern China.

The time series also indicates that EVI is less affected by snow than NDVI and works better in maize cropland and degraded grassland in semi-arid regions.

Significant variation in the values of vegetation indices (EVI, NDVI) was observed during 2004–2006, and this variation appeared to correspond to variation in GPP (Fig. 7). There was distinct difference, however, in the VI-GPP relationships between EVI and NDVI. In both maize cropland and degraded grassland, EVI had a stronger linear relationship with GPP than NDVI (Fig. 7). There were strong linear correlations between the two vegetation indices and GPP for maize cropland:  $R^2 = 0.817$  for NDVI, and  $R^2 = 0.822$  for EVI. For the degraded grassland site, because of low vegetation coverage, the linear relationship was not as good as maize cropland; however, EVI correlated well with GPP having an  $R^2 = 0.770$ , while NDVI had an  $R^2 = 0.696$ . The results were all significant at 5% level.

#### 4.3. Simulation of the VPM

Simulation of the VPM model was completed using vegetation indices (EVI, LSWI) derived from the 8-day MODIS Surface Reflectance Product and site-specific data for temperature and PAR for 2004–2006. The seasonal dynamics of predicted GPP ( $GPP_{pred}$ ) from the VPM model were compared with the estimated GPP ( $GPP_{est}$ ) data for 8-day intervals (Fig. 8). The seasonal dynamics of  $GPP_{pred}$  for both the maize cropland and the degraded grassland agreed well with those of  $GPP_{est}$  in terms of phase and magnitude.

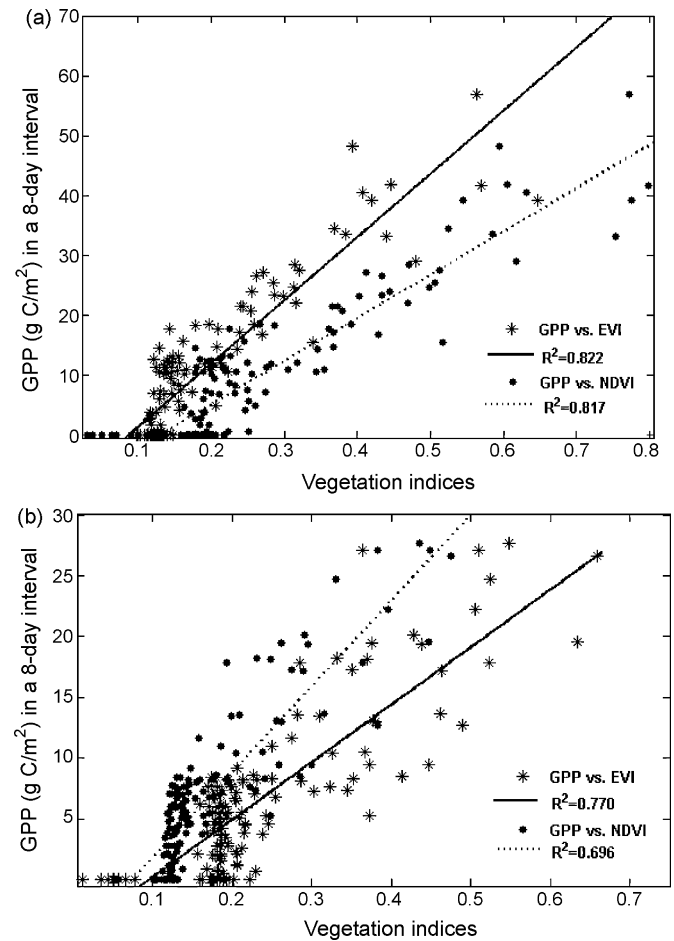


**Fig. 7.** Simple linear regression analyses between GPP and vegetation indices (NDVI, EVI), with 3-year data for (a) maize cropland and (b) degraded grassland. The two semi-arid ecosystems are in Tongyu, northeastern China. Solid line is regression analysis between GPP and EVI and dashed line is regression analysis between GPP and NDVI.

The simple linear regression model also shows high correlation between  $GPP_{pred}$  and  $GPP_{est}$  (Fig. 9). Discrepancies exist between  $GPP_{pred}$  and  $GPP_{est}$  in a few 8-day periods. For instance, several  $GPP_{pred}$  values were lower than  $GPP_{est}$  values, especially in degraded grassland, at the beginning of the growing season. For maize cropland, annual  $GPP_{est}$  from the flux estimation was 392, 504 and 437  $gC/m^2$  in 2004, 2005 and 2006, respectively. Annual  $GPP_{pred}$  from the VPM model was 310, 464 and 360  $gC/m^2$ . Annual  $GPP_{est}$  for degraded grassland was 292  $gC/m^2$  in 2004, 331  $gC/m^2$  in 2005 and 291  $gC/m^2$  in 2006, while annual  $GPP_{pred}$  for degraded grassland was 252  $gC/m^2$  in 2004, 298  $gC/m^2$  in 2005 and 258  $gC/m^2$  in 2006.

The results of the simple linear regression analyses between  $GPP_{pred}$  and  $GPP_{est}$  for maize cropland and degraded grassland indicate that the VPM model can predict GPP well in both humid years and dry years at the semi-arid region in Tongyu, northeastern China (Fig. 9). Data points within the plant-growing season, instead of yearly data, have been used for regression analysis, and these show a strong correlation between the  $GPP_{pred}$  and  $GPP_{est}$  of degraded grassland ( $R^2 = 0.805$ ) and a stronger correlation for maize cropland ( $R^2 = 0.839$ ). The results were significant at 5% level.

There were discrepancies between  $GPP_{est}$  and  $GPP_{pred}$  in a few 8-day periods. The large discrepancies can be attributed in part to prediction error of  $GPP_{pred}$  from the VPM model and in part to estimation error of  $GPP_{est}$  (Xiao et al., 2004a). The simulation error in the VPM model came from the input climate data and vege-

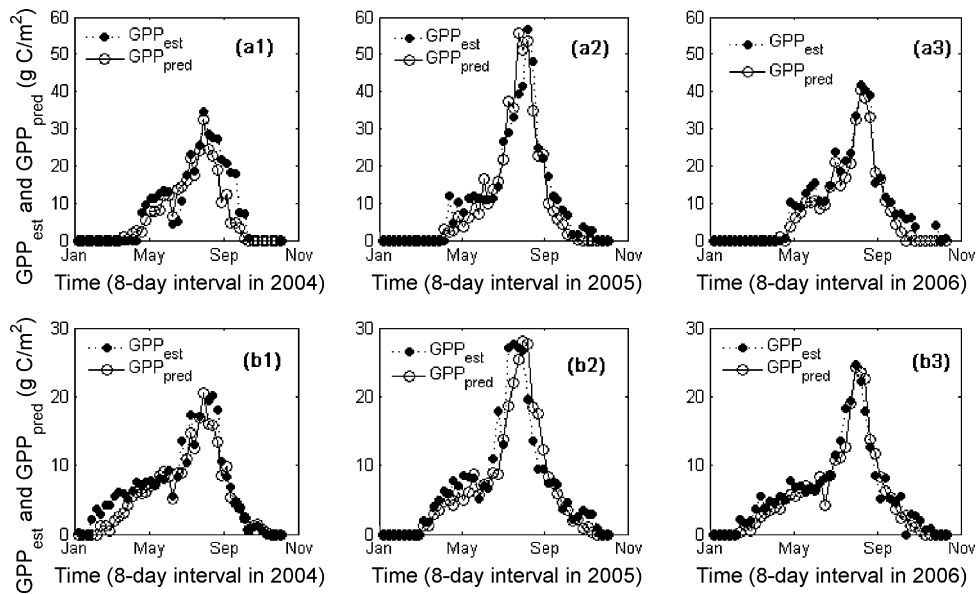


**Fig. 8.** Comparison of the seasonal dynamics between the estimated gross primary production ( $GPP_{est}$ ) from tower data and predicted GPP ( $GPP_{pred}$ ) by the VPM model during 2004–2006 at (a) maize cropland and (b) degraded grassland. The two semi-arid ecosystems are in Tongyu, northeastern China.

tation indices. There was a distinct influence of temperature on crop growth in early spring, but in the VPM model we used 8-day mean daytime temperature, which in some cases introduced error. Vegetation indices (EVI, NDVI, and LSWI) were derived from

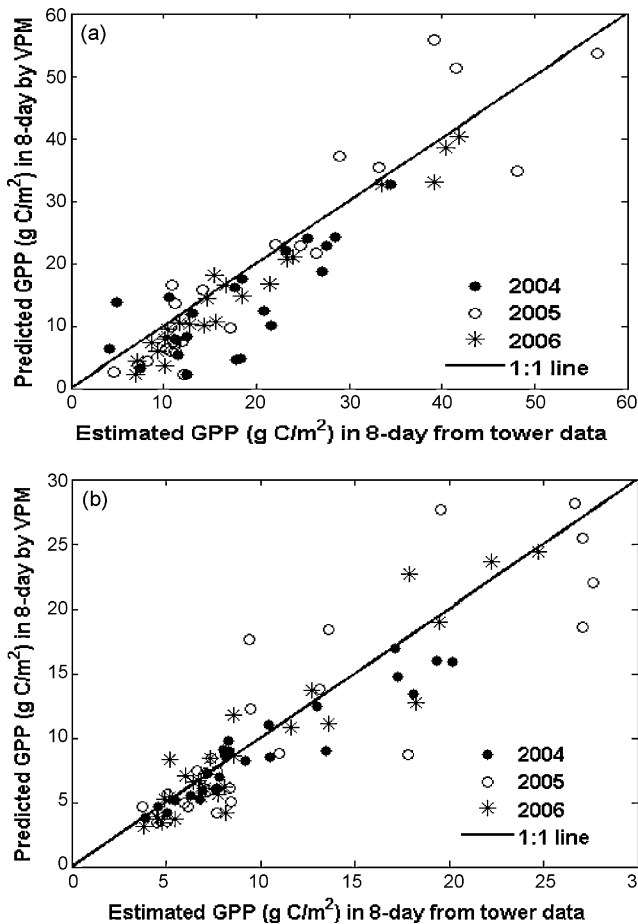


**Fig. 9.** A simple linear regression analyses between predicted gross primary production (GPP) by the VPM model and estimate GPP from the tower data during 2004–2006 at (a) maize cropland and (b) degraded grassland. The two semi-arid ecosystems are in Tongyu, northeastern China.

8-day MODIS imagery lacking BRDF correction, which results in unidentifiable overestimation and underestimation.

A number of Eddy Covariance flux sites with open-path analyzers have observed small apparent  $CO_2$  uptake outside the growing season (Burba et al., 2008). In this study, there were some small negative  $CO_2$  fluxes and physiologically unreasonable winter  $GPP_{est}$  appeared in Fig. 5. Burba et al. (2008) found that apparent off-season  $CO_2$  uptake can be attributed to open-path analyzers specifically. The difference between instrument surface temperature and the ambient temperature could lead to sensible heat fluxes inside the open-path cell which are different from those in the ambient air, thus affecting the  $CO_2$  densities measured in the instrument path. In this study, the off-season  $CO_2$  uptake was not eliminated with the traditionally computed WPL term.

Modeling gross primary production of maize cropland and degraded grassland in northeastern China, we found two significant results: (1) The VPM model has now been evaluated and applied in maize cropland and degraded grassland in semi-arid regions. The comparison between  $GPP_{est}$  and  $GPP_{pred}$  showed that the GPP predicted by the VPM model agreed well with estimated GPP, which indicates the potential of the satellite-driven VPM model for up-scaling GPP in semi-arid ecosystems. (2) For semi-arid regions, EVI had a stronger linear relationship with GPP than did NDVI. As vegetation indices can be used to characterize vegetation conditions and detect information of aridification, many studies have used NDVI to describe vegetation in arid and semi-arid regions in northeastern China (Zhang et al., 2005), but this study demonstrated the improvement of EVI over NDVI for both maize cropland and degraded grassland in a semi-arid area. As a hypothesis in the VPM model, EVI and the relationship between chlorophyll and  $FPAR_{chl}$  can produce more information about vegetation structure-related dynamics and canopy condition changes such as changes in proportion of photosynthetic/non-photosynthetic biomass or pigment content.

In summary, this study evaluated the potential of the VPM model for estimating GPP in semi-arid regions and biophysical performance of vegetation indices (EVI, NDVI, and LSWI). The results have significant implications for remote sensing analyses of maize cropland and degraded grassland in semi-arid regions. Estimation of GPP and its seasonal dynamics is a first step in the study of the carbon cycle of the semi-arid region in northeastern China, and

further research is needed to understand the terrestrial biosphere interaction in arid and semi-arid regions.

## Acknowledgements

The work has been supported by grants from the China Ministry of Science and Technology (2006CB400500) and NASA Land Cover and Land Use program (NEWS 2004 NRA: NN-H-04-Z-YS-005-N). We thank the data management of RCE-TEA for data collection at the flux tower sites and NASA for access to MODIS data. We also acknowledge and thank two reviewers for their comments and insight and Joshua Kalfas for proof-reading and improving the use of English in this manuscript.

## References

- Baldocchi, D., Falge, E., Gu, L., Olson, R., Hollinger, D., Running, S., Anthoni, P., Bernhofer, C., Davis, K., Evans, R., 2001. Fluxnet: a new tool to study the temporal and spatial variability of ecosystem-scale carbon dioxide, water vapor, and energy flux densities. *Bulletin of the American Meteorological Society* 82, 2415–2434.
- Burba, G.G., Mcdermitt, D.K., Grelle, A., Anderson, D.J., Xu, L., 2008. Addressing the influence of instrument surface heat exchange on the measurements of CO<sub>2</sub> flux from open-path gas analyzers. *Global Change Biology* 14, 1854–1876.
- Elmar, M., Veenendaal, O.K.J.L., 2004. Seasonal variation in energy fluxes and carbon dioxide exchange for a broad-leaved semi-arid savanna (Mopane woodland) in Southern Africa. *Global Change Biology* 10, 318–328.
- Evenari, M., Noy-Meir, I., Goodall, D.W., 1985. *Hot Deserts and Arid Shrublands*. Elsevier Science Publishers, 366 pp.
- Falge, E., Baldocchi, D., Olson, R., Anthoni, P., Aubinet, M., Bernhofer, C., Burba, G., Ceulemans, R., Clement, R., Dolman, H., Granier, A., Gross, P., Grünwald, T., Hollinger, D., Jensen, N.-O., Katul, G., Keronen, P., Kowalski, A., Ta Lai, C., Law, B.E., Meyers, T., Moncrieff, J., Moors, E., William Munger, J., Pilegaard, K., Rannik, Ü., Rebmann, C., Suyker, A., Tenhunen, J., Tu, K., Verma, S., Vesala, T., Wilson, K., Wofsy, S., 2001a. Gap filling strategies for long term energy flux data sets. *Agricultural and Forest Meteorology* 107, 71–77.
- Falge, E., Baldocchi, D., Olson, R., Anthoni, P., Aubinet, M., Bernhofer, C., Burba, G., Ceulemans, R., Clement, R., Dolman, H., Granier, A., Gross, P., Grünwald, T., Hollinger, D., Jensen, N.-O., Katul, G., Keronen, P., Kowalski, A., Ta Lai, C., Law, B.E., Meyers, T., Moncrieff, J., Moors, E., William Munger, J., Pilegaard, K., Rannik, Ü., Rebmann, C., Suyker, A., Tenhunen, J., Tu, K., Verma, S., Vesala, T., Wilson, K., Wofsy, S., 2001b. Gap filling strategies for defensible annual sums of net ecosystem exchange. *Agricultural and Forest Meteorology* 107, 43–69.
- Friend, A.D., Stevens, A.K., Knox, R.G., Cannell, M.G.R., 1997. A process-based, terrestrial biosphere model of ecosystem dynamics (Hybrid v3.0). *Ecological Modelling* 95, 249–287.
- Fu, C.B., Wen, G., 2002. Several issues on aridification in the northern China. *Climatic and Environmental Research* 7, 22–29 (in Chinese).
- Fu, C.B., An, Z.S., 2002. Study of aridification in northern China—a global change issue forcing directly the demand of Nation. *Earth Science Frontiers* 9, 271–275 (in Chinese).
- Goetz, S.J., Prince, S.D., Goward, S.N., Thawley, M.M., Small, J., 1999. Satellite remote sensing of primary production: an improved production efficiency modeling approach. *Ecological Modelling* 122, 239–255.
- Goodrich, D.C., Chehbouni, A., Goff, B., MacNish, B., Maddock, T., Moran, S., Shuttleworth, W.J., Williams, D.G., Watts, C., Hipps, L.H., Cooper, D.I., Schieldge, J., Kerr, Y.H., Arias, H., Kirkland, M., Carlos, R., Cayrol, P., Kepner, W., Jones, B., Avissar, R., Begue, A., Bonnefond, J.M., Boulet, G., Branan, B., Brunel, J.P., Chen, L.C., Clarke, T., Davis, M.R., DeBruin, H., Dedieu, G., Elguero, E., Eichinger, W.E., Everitt, J., Garatua-Payan, J., Gempko, V.L., Gupta, H., Harlow, C., Hartogensis, O., Helfert, M., Holifield, C., Hymer, D., Kahle, A., Keefer, T., Krishnamoorthy, S., Lhomme, J.P., Lagouarde, J.P., Lo Seen, D., Luquet, D., Marsset, R., Monteny, B., Ni, W., Nouvelon, Y., Pinker, R., Peters, C., Pool, D., Qi, J., Rambal, S., Rodriguez, J., Santiago, F., Sano, E., Schaeffer, S.M., Schulte, M., Scott, R., Shao, X., Snyder, K.A., Sorooshian, S., Unkrich, C.L., Whitaker, M., Yucel, I., 2000. Preface paper to the semi-arid land-surface-atmosphere (SALSA) program special issue. *Agricultural and Forest Meteorology* 105, 3–20.
- Heinsch, F.A., Reeves, M., Votava, P., Kang, S., Milesi, C., Zhao, M., Glassy, J., Jolly, W.M., Loehman, R., Bowker, C.F., Kimball, J.S., Nemani, R.R., Running, S.W., 2003. *User's Guide: GPP and NPP (MOD17A2/A3) Products NASA MODIS Land Algorithm: Version 2.0*.
- Hu, Y.Q., Gao, X.Y., 1994. Some new understandings of processes at the land surface in arid area from the HEIFE. *Acta Meteorologica Sinica* 52, 285–296.
- Huete, A.R., Liu, H.Q., Batchily, K., van Leeuwen, W., 1997. A comparison of vegetation indices over a global set of TM images for EOS-MODIS. *Remote Sensing of Environment* 59, 440–451.
- Jiang, J.-f., Yan, X.-d., Huang, Y., Jiang, J.-f., Yan, X.-d., Huang, Y., Guo, W.-d., Liu, H.-z., 2007. Simulation of CO<sub>2</sub> and sensible/latent heat fluxes exchange between land surface and atmosphere over cropland and grassland in semi-arid region, China. *Journal of Forestry Research* 18, 114–118.
- Laura, F., Huenneke, J.P.A.M.R.W.H.S., 2002. Desertification alters patterns of above-ground net primary production in Chihuahuan ecosystems. *Global Change Biology* 8, 247–264.
- Li, Z., Yu, G., Xiao, X., Li, Y., Zhao, X., Ren, C., Zhang, L., Fu, Y., 2007. Modeling gross primary production of alpine ecosystems in the Tibetan Plateau using MODIS images and climate data. *Remote Sensing of Environment* 107, 510–519.
- Liu, H., Tu, G., Fu, C., Shi, L., 2008. Three-year variations of water, energy and CO<sub>2</sub> fluxes of cropland and degraded grassland surfaces in a semi-arid area of North-eastern China. *Advances in Atmospheric Sciences* 25, 1009–1020.
- Lu, D.R., Chen, Z.Z., Chen, J.Y., 2005. Study on soil-vegetation-atmosphere interaction in inner-Mongolia semi-aridgrassland. *Acta Meteorologica Sinica* 65, 571–593.
- Ma, Y.-m., Yao, T.-d., Wang, J.-m., 2006. Experimental study of energy and water cycle in tibetan plateau—the progress introduction on the study of GAME/Tibet and CAMP/Tibet. *Plateau Meteorology* 25, 344–351.
- Mahadevan, P., Wofsy, S.C., Matross, D.M., Xiao, X., Dunn, A.L., Lin, J.C., Gerbig, C., Munger, J.W., Chow, V.Y., Gottlieb, E.W., 2008. A satellite-based biosphere parameterization for net ecosystem CO<sub>2</sub> exchange: vegetation photosynthesis and respiration model (VPRM). *Global Biogeochemical Cycles* 22.
- Raich, J.W., Rastetter, E.B., Melillo, J.M., Kicklighter, D.W., Steudler, P.A., Peterson, B.J., Grace, A.L., Moore III, B., Vorosmarty, C.J., 1991. Potential net primary productivity in South-America—application of a global-model. *Ecological Applications* 1, 399–429.
- Ruimy, A., Dedieu, G., Saugier, B., 1996. TURC: a diagnostic model of continental gross primary productivity and net primary productivity. *Global Biogeochemical Cycles* 10.
- Ruimy, A., Jarvis, P.G., Baldocchi, D.D., Saugier, B., 1995. CO<sub>2</sub> fluxes over plant canopies and solar radiation: a review. *Advances in Ecological Research*.
- Tucker, C.J., 1979. Red and photographic infrared linear combinations for monitoring vegetation. *Remote Sensing of Environment (United States)* 8, 127–150.
- Verhoef, A., Allen, S.J., Lloyd, C.R., 1999. Seasonal variation of surface energy balance over two Sahelian surfaces. *International Journal of Climatology* 19, 1267–1277.
- Wang, J., Mitsuta, Y., 1991. Turbulence structure and transfer characteristics in the surface layer of the HEIFE Gobi area. *Journal of the Meteorological Society of Japan* 69, 587–593.
- Wesfall, J., Stumm, 1980. *The hydrosphere*. In: Hutzinger, O. (Ed.), *The Handbook of Environmental Chemistry*. Springer-Verlag.
- Wofsy, S.C., Goulden, M.L., Munger, J.W., Fan, S.M., Bakwin, P.S., Daube, B.C., Bassow, S.L., Bazzaz, F.A., 1993. Net exchange of CO<sub>2</sub> in a mid-latitude forest. *Science* 260, 1314–1317, doi:10.1126/science.260.5112.1314.
- Xiao, X., Boles, S., Liu, J., Zhuang, D., Liu, M., 2002. Characterization of forest types in Northeastern China, using multi-temporal SPOT-4 VEGETATION sensor data. *Remote Sensing of Environment* 82, 335–348.
- Xiao, X., Zhang, Q., Hollinger, D., Aber, J., Moore, B., 2005a. Modeling gross primary production of an evergreen needleleaf forest using modis and climate data. *Ecological Applications* 15, 954–969, doi:10.1890/04-0470.
- Xiao, X., Hollinger, D., Aber, J., Goltz, M., Davidson, E.A., Zhang, Q., Moore, B., 2004a. Satellite-based modeling of gross primary production in an evergreen needleleaf forest. *Remote Sensing of Environment* 89, 519–534.
- Xiao, X., Zhang, Q., Braswell, B., Urbanski, S., Boles, S., Wofsy, S., Moore, B., Ojima, D., 2004b. Modeling gross primary production of temperate deciduous broadleaf forest using satellite images and climate data. *Remote Sensing of Environment* 91, 256–270.
- Xiao, X., Zhang, Q., Saleska, S., Hutyrá, L., De Camargo, P., Wofsy, S., Frolking, S., Boles, S., Keller, M., Moore, B., 2005b. Satellite-based modeling of gross primary production in a seasonally moist tropical evergreen forest. *Remote Sensing of Environment* 94, 105–122.
- Xu, X., Zhou, M., Chen, J., Bian, L., Zhang, G.-z., Liu, H.-z., Li, S.-m., Zhang, H.-s., Zhao, Y.-j., Suolongduoji, Wang, J.-z., 2002. A comprehensive physical pattern of land-air dynamic and thermal structure on the Qinghai-Xizang Plateau. *Science in China Series D: Earth Sciences* 45, 577–594.
- Zhang, J.-y., Dong, W.-j., Wu, L.-y., Wei, J.-f., Chen, P.-y., Dong-Kyou, LEE, 2005. Impact of land use changes on surface warming in China. *Advances in Atmospheric Sciences* 22, 343–348.
- Zhang, Q.G., Wei, G.A., Huang, R.H., 2001. Observation and study of atmospheric drag coefficients in Dunhuang. *Science in China (D)* 31, 783–792.